

# Upper mantle seismic anisotropy resulting from pressure-induced slip transition in olivine

Haemyeong Jung<sup>1\*</sup>, Won Mo<sup>1</sup> and Harry W. Green<sup>2\*</sup>

**Seismic anisotropy in the oceanic lithosphere results from flow-induced crystallographic preferred orientation of dry olivine during lithosphere creation. Recent experiments, however, showed that high water activity changes the flow mechanisms of olivine and hence the crystallographic preferred orientation, better explaining the seismic anisotropy in the mantle wedge above subduction zones. Whether changes in the crystallographic preferred orientation of olivine are unique to the effects of water has become controversial and is critical to resolve. Here we report low-stress, high-strain experiments on typical dry mantle rock at high pressures and temperatures, showing that at ~3 GPa, pressure induces the same profound transition in olivine crystallographic preferred orientation that is produced by high water activity at lower pressure. One important consequence for global tectonics is that alignment of fast seismic waves parallel to trenches beneath subducting slabs probably reflects entrainment of sub-lithospheric mantle in the direction of subduction, rather than trench-parallel flow as interpreted at present. From the large variety of crystallographic preferred orientations in olivine in both experiments and natural rocks, we infer that in addition to the pressure-induced changes in olivine slip systems implied here, there are probably further changes in slip systems at higher pressure and temperature.**

Seismic anisotropy is a powerful tool for unravelling tectonics within the Earth's mantle. For 30 years, it has been understood that the prominent seismic anisotropy of the oceanic lithosphere (cold, strong, uppermost layer of the mantle) is a result of strong deformation of olivine during the formation of the lithosphere at oceanic spreading centres<sup>1</sup>. Other areas of the upper mantle showing significant seismic anisotropy have been interpreted assuming that the flow mechanisms and crystallographic preferred orientation (CPO) of olivine are always the same<sup>2,3</sup>. Recently, however, it has been demonstrated<sup>4</sup> that at high fugacity of H<sub>2</sub>O, the easiest slip direction in olivine changes from [100] to [001] and several different CPOs can be produced in the laboratory<sup>4-6</sup>, some of which have natural analogues<sup>7-10</sup>, and several of which, when applied to understand seismic anisotropy in the upper mantle, imply a different flow geometry than that obtained previously on the basis of the assumption that the flow mechanism does not change with conditions. This discovery potentially opened the door to 'prospecting' for H<sub>2</sub>O in the mantle by measuring the seismic anisotropy<sup>3,11,12</sup>.

Further experimentation at high pressure and theoretical calculations, however, have complicated the issue by finding the same switch in the olivine easy-slip direction (from [100] to [001]) in a dry environment at pressures in excess of 3 GPa (refs 13–15). A controversy has ensued because it has not been demonstrated to the satisfaction of the community that the more recent experiments were both dry and conducted under sufficiently low stresses to be relevant to interpretation of the Earth<sup>5,16</sup>. We report here resolution of this controversy using the only deformation apparatus at present that can conduct low-stress experiments at pressures in excess of 3 GPa (see the Methods section). We show below that there is, indeed, a pressure-induced change in olivine slip systems that occurs at approximately 3 GPa in a demonstrably dry environment, with significant implications for global tectonics.

## Experimental results

We have conducted a series of four experiments, all at 1,300 °C, at pressures of 2.5, 3.1, 3.1 and 3.6 GPa (Table 1). Water was not detectable in olivine of the starting material (harzburgite) and analysis of several different areas of all samples showed that only one specimen contained detectable H<sub>2</sub>O (Fig. 1). The values of the stresses measured for these experiments are in most cases lower than those calculated for the original wet experiments of Jung and Karato<sup>4</sup> and shear strains of these samples are larger than those of any of the other studies involved<sup>4,13,14,17,18</sup>.

Figure 2 shows that pressure has a marked effect on the CPO of olivine. At 2.5 GPa (Fig. 2a), the [100] axes of olivine are preferentially subparallel to the shear direction and the maximum of [010] axes is subparallel to the shear-plane normal, yielding the type-A CPO (ref. 5). In contrast, at 3.1 GPa (Fig. 2b) and 3.6 GPa (Fig. 2c) there is a paucity of [100] axes in the shear direction whereas [001] now has significant concentration in the shear direction; [010] axes remain concentrated subnormal to the shear plane, yielding the type-B CPO (ref. 5). The fourth sample of this series, deformed at 3.1 GPa and showing a water content of 90 p.p.m. H/Si after deformation (Fig. 1), showed a similar type-B CPO.

The change in active olivine slip systems is even more strikingly shown in the inverse pole figures of Fig. 3. At  $P = 2.5$  GPa, there is a very strong maximum of the shear direction parallel to [100] and a comparable maximum of the shear-plane normal quasi-parallel to [010], indicating that most strain is accomplished by slip on (010) in the [100] direction. At 3.1 GPa, however, the large maximum of the shear direction parallel to [100] is completely gone and replaced by a strong maximum of the shear direction parallel to [001]; the maximum of the shear-plane normal subparallel to [010] remains, indicating that the dominant slip plane remains (010) but that the easy-glide direction has switched profoundly from [100] to

<sup>1</sup>School of Earth and Environmental Sciences, Seoul National University, 311 Ho, 25-1 Dong, San 56-1, Sillim-dong, Gwanak-gu, Seoul 151-747, Korea,

<sup>2</sup>Institute of Geophysics and Planetary Physics and Department of Earth Sciences, University of California, Riverside, California 92521, USA.

\*e-mail: hjung@snu.ac.kr; harry.green@ucr.edu.

**Table 1 | Experimental conditions and results.**

Run No.	<i>P</i> (GPa)	<i>T</i> <sub>1</sub> (°C)	<i>T</i> <sub>2</sub> (°C)	Fabric type	Shear strain ( $\gamma$ )	Differential stress (MPa)	Strain rate (s <sup>-1</sup> )	Water content (p.p.m. H/Si)
GB328	2.5	1,290	1,300	A	3.0 ± 0.3	120	6 × 10 <sup>-5</sup>	UD
GB323	3.1	1,270	1,300	B	3.0 ± 0.3	150	2 × 10 <sup>-5</sup>	UD
GB325	3.1	1,270	1,300	B	4.0 ± 0.5	250	6 × 10 <sup>-5</sup>	90 ± 30
GB335	3.6	1,300	1,290	B	6.0 ± 0.5	390	6 × 10 <sup>-5</sup>	UD

*T*<sub>1</sub> and *T*<sub>2</sub> represent the temperature near the top and bottom of the specimen, respectively. Differential stress was measured with an external load cell. Water content was measured by the Nicolet 6700 FTIR spectrometer with a continuum infrared microscope and was estimated using the Paterson calibration<sup>27</sup>. UD refers to 'undetectable from the FTIR'. See Fig. 1 for FTIR spectra.

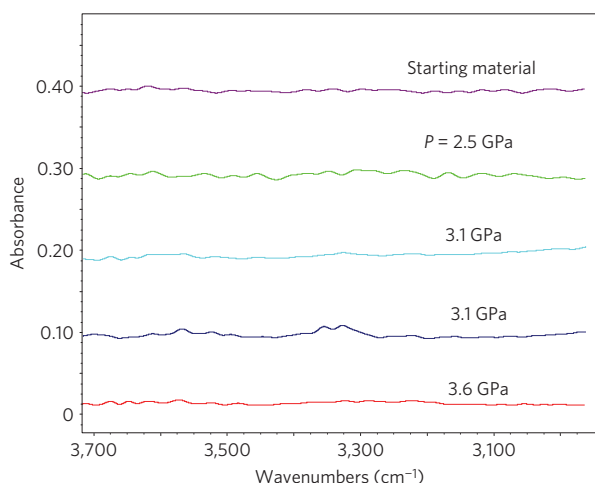


**Figure 1 | Unpolarized FTIR spectra of olivine before and after the experiments.** The infrared beam size of 30 μm × 30 μm was used in the transmission mode. These data show that water was not detectable in the starting material and that three out of four samples were equally dry after deformation; the exception, one of those at 3.1 GPa, contained 90 ± 30 p.p.m. H/Si, showing O–H stretching bands at 3,329, 3,357 and 3,570 cm<sup>-1</sup>.

[001]. At 3.6 GPa, the pattern remains basically the same, but the strength of the shear direction maximum has decreased whereas the slip-plane normal maximum has greatly strengthened. This observation, coupled with the CPO for [001] in Fig. 2, suggests that the strain in this specimen may have a significant component of shortening normal to the shear plane, with some contribution from [100] slip. This would also be consistent with the greater strength exhibited by this specimen (Table 1) having resulted in subordinate activation of [100].

These results show that, even at low stresses, pressure has a marked effect on the CPO of dry olivine (Fig. 2). The inverse pole figures show clearly that the dominant slip system in olivine changed markedly between 2.5 and 3.1 GPa (Fig. 3). The implication is that the pressure dependence of the critical resolved shear stress for slip along the [100] direction on the (010) plane is greater than that for slip along [001] on the same plane, resulting in a crossover around 3 GPa. As a consequence, the easiest glide plane remains (010), but at higher pressure slip occurs more easily in the [001] direction than in the [100] direction. High activity of H<sub>2</sub>O lowers this crossover by 1–2 GPa (ref. 4).

The seismic anisotropy corresponding to these fabrics is shown in Fig. 4. The velocity distribution figures are oriented looking down on the shear plane with the shear direction east–west to compare hypothetical seismic data for each type of CPO, presuming a horizontal shear plane in the Earth and quasi-vertical shear-wave arrivals. Both *P*-wave seismic velocity and *S*-wave polarization anisotropy are calculated from the CPO of olivine (Fig. 2). At

*P* = 2.5 GPa, the seismically fast [100] axes are subparallel to the shear direction. Thus, *P*-waves propagate with the highest velocity in the shear direction. However, at all pressures above 3 GPa, the [100] axes of olivine are almost normal to the shear direction, in the shear plane. Thus, in this case *P*-waves propagate fastest perpendicular to the shear direction. *V*<sub>p</sub> anisotropy and maximum *AV*<sub>s</sub> anisotropy (Fig. 4) are weak for the large shear strains obtained in this study, suggesting that low seismic anisotropies in the upper mantle may be a result of weak olivine CPO development at higher pressure. It is noteworthy that the polarization direction of the fast *S*-wave (*V*<sub>s1</sub> polarization) at *P* = 3.1 GPa (type-B) is almost perpendicular to the shear direction in the shear plane.

#### Comparison of our results with previous studies

Couvy *et al.*<sup>13</sup> conducted simple shear deformation experiments on Fe-free olivine (forsterite) using multi-anvil apparatus at *P* = 11 GPa and *T* = 1,400 °C. Under these conditions, they found olivine fabrics similar to the C-type fabric<sup>4</sup> and suggested that pressure changes the slip systems of olivine. Unfortunately, there are some difficulties with the results of their pioneering experiments: (1) shear strain was too small ~0.1–0.3 to demonstrate conclusively the change in CPO of olivine; (2) stress varied during individual experiments from ~1,500 MPa at the beginning to ~100 MPa at the end, obscuring the effect of stress on their results; (3) the water content of olivine at the end of their experiments was high ~850–2,200 p.p.m. H/Si, raising the possibility that the change in CPO was due to H<sub>2</sub>O rather than pressure. Their results (C-type CPO) are different from ours (B-type CPO), presumably because of one or more of these three factors or the higher pressure of their experiments. Raterron *et al.*<sup>14</sup> conducted two deformation experiments on single-crystal forsterite at *P* = 2.1–7.5 GPa and *T* = 1,100–1,404 °C using a Deformation-DIA apparatus and reported that the dominant slip direction of forsterite changes from **b** = [100] to [001] between *P* = 3 and 7 GPa. However, the stress of their experiments was high ~300–1,800 MPa, leaving ambiguous whether the change in slip system was a pressure effect or a stress effect<sup>16,19</sup>. Moreover, both of these previous studies were conducted on Fe-free olivine, which does not always proxy accurately for the Fe-bearing olivine of the Earth's mantle. The present results remove these ambiguities and demonstrate the effect of pressure on the CPO of olivine of mantle composition.

#### Implications for seismic anisotropy

Concerning application of this discovery to the Earth, seismic anisotropy caused by the CPO of dry olivine under high pressure (Fig. 4) must be significantly different from that under low pressure<sup>4,17</sup>. On the basis of the results in this study, flow of olivine-bearing rocks under dry conditions at depths of ~80–100 km and temperatures reasonably close to those of our experiments (1,300 °C) will retain the (010) plane parallel to the flow plane but will concentrate olivine [100] axes normal to the flow direction rather than parallel to it. For example, type-B CPO produced in dry olivine strongly suggests that seismic anisotropy indicative of

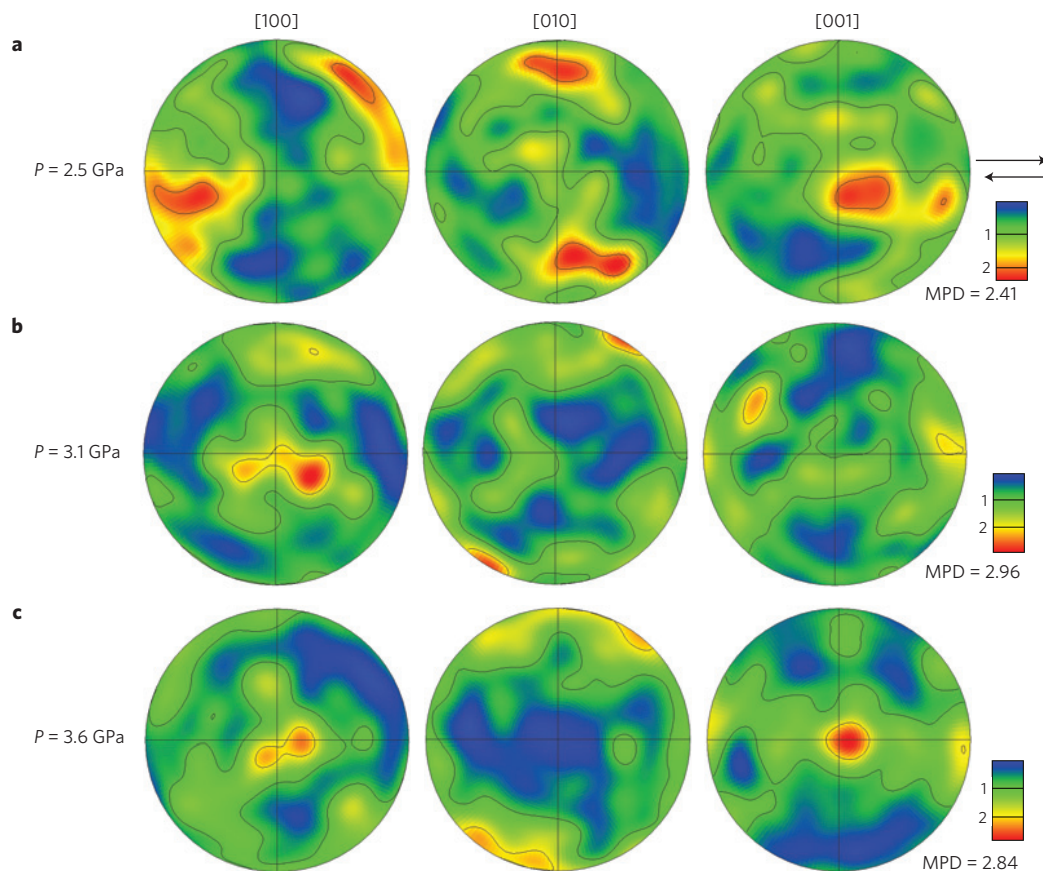


**Figure 2 | Pole figures: Equal-area upper hemisphere projections of olivine crystal axis distributions.** The arrows show the shear sense, and the north-south poles correspond to the shear-plane normal. The contours correspond to multiples of a uniform distribution of data points. In all three specimens represented here, the water content was undetectable. **a**,  $T = 1,300\text{ }^{\circ}\text{C}$ ,  $\gamma = 3$ , differential stress = 120 MPa. **b**,  $T = 1,300\text{ }^{\circ}\text{C}$ ,  $\gamma = 3$ , differential stress = 150 MPa. **c**,  $T = 1,300\text{ }^{\circ}\text{C}$ ,  $\gamma = 6$ , differential stress = 390 MPa. A half-width of  $20^{\circ}$  was used to draw the pole figures. MPD = maximum pole figure density.

trench-parallel fast seismic waves observed beneath the down-going plate in many subduction zones<sup>20–22</sup> indicates entrainment of the mantle below the slab in the direction of subduction, rather than reflecting trench-parallel flow<sup>21,22</sup>. On the other hand, the mantle wedge above a subducting slab can be expected to be ‘wet’ as a result of fluids released by the dehydration of hydrous minerals within the slab. Such fluids, expelled upward from the slab, migrate through the mantle wedge down the gravitational and pressure gradients and up the temperature gradient, where they trigger hydrous melting of the wedge, yielding arc and back-arc volcanism. Thus, type-B CPO of olivine is likely to be present in both locations—the former induced by high pressure and the latter induced by high  $\text{H}_2\text{O}$  fugacity at lower pressure. The fact that we cannot be sure that the mantle wedge is ‘wet’ everywhere, however, introduces ambiguity into interpretation of the seismic anisotropy of shallow arc and back-arc regions.

The type-B CPO of olivine has been observed in natural rocks: for example, deformed peridotites from Mount Higashi Akaishi, Japan<sup>7</sup>, Cima di Gagnone, Switzerland<sup>8</sup> and Val Malenco, Italy<sup>9</sup>. Our results show that the type-B CPO of olivine in natural rocks could be the result of either a water-induced fabric transition or a pressure-induced fabric transition. Distinguishing between the two origins must be based on indicators of a hydrous environment during flow—such as microstructural indications that clinohumite or phlogopite are involved with the foliation rather than being an overprint as is usually the case.

There are other CPOs of olivine known, both in the wet experiments and in nature, that are not addressed here and remain

loose ends in understanding the pressure/temperature dependence of olivine CPO. In particular, the C-type CPO ([100] normal to foliation and [001] parallel to the lineation in the foliation plane) that is found in famous locations such as Alpe Arami, Switzerland<sup>23</sup>, and the Western Gneiss terrane, Norway<sup>10</sup>, was found in the highest pressure experiments discussed here<sup>13</sup> and may reflect a still higher pressure slip-system transition in olivine in which [001] remains the easy-glide direction but the preferred glide plane becomes (100) (see Supplementary Information). In addition, the A-type CPO has been reported from kimberlite xenoliths<sup>24</sup>, which probably reflects a temperature dependence of slip in olivine that extends the A-type CPO to greater depths at higher temperatures or, alternatively, could reflect a technical problem in those measurements (see Supplementary Information, Note).

In summary, the seismic anisotropy of the mantle wedge above subducting slabs at a depth of  $\sim 75$  km or less can most likely be attributed to the type-B olivine CPO induced by the presence of water, although it remains possible that in some instances such seismic anisotropy could be the result of type-A CPO produced by flow of dry olivine. Elsewhere in the mantle at these depths, type-A CPO is expected from dry olivine unless there is independent evidence suggesting involvement of  $\text{H}_2\text{O}$ . In contrast, at depths greater than 80–90 km in subduction zone environments, seismic anisotropy can most likely be attributed to type-B olivine CPO, independent of water content. Moreover, Jung and Karato<sup>4</sup> identified other CPOs, some of which (type-C and -E) have natural equivalents<sup>9,10</sup>, that they also interpreted as being due to high  $\text{H}_2\text{O}$  fugacity. Our experiments do not address these CPOs; more

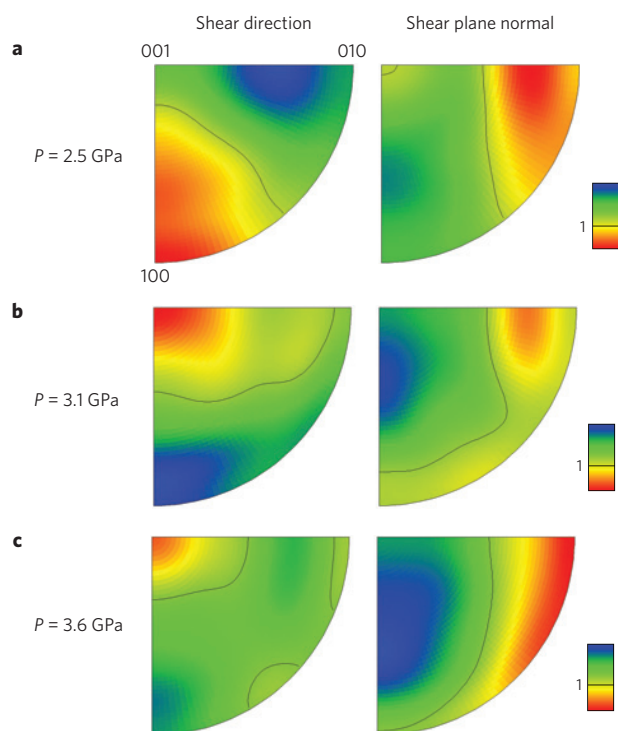


**Figure 3 | Inverse pole figures of the same data as shown in Fig. 2.** The figures plot and contour the shear direction and the shear-plane normal as seen from every crystal measured. The colour coding represents the density of data points; the contours correspond to multiples of a uniform distribution. The concentration of the shear direction at 2.5 GPa is strongly parallel to [100]; it changes profoundly to parallel to [001] at 3.1 GPa and above, indicating that the dominant slip system changes from (010)[100] to (010)[001] between 2.5 GPa and 3.1 GPa. A half-width of  $30^\circ$  was used to draw the inverse pole figures.

experiments will be necessary to understand the complete effects of pressure, temperature and water on the CPO of olivine under higher pressure, and hence the full spectrum of possibilities for interpretation of seismic anisotropy.

## Methods

We prepared a powder of  $\sim 96\%$  natural olivine ( $\text{Mg}_{0.9}\text{Fe}_{0.1}\text{SiO}_4$ , 3% enstatite and  $\sim 1\%$  spinel) that was subjected to commercial isostatic hot pressing at 200 MPa and  $1,400^\circ\text{C}$ , yielding a synthetic harzburgite with average grain size of  $\sim 50\ \mu\text{m}$ . For these experiments, we wished to, as much as possible, replicate the experiments of Jung and Karato<sup>4</sup> except for establishing dry conditions and higher pressures; a thin slice of the starting material ( $\sim 300\ \mu\text{m}$  thick) was sandwiched between two  $\text{Al}_2\text{O}_3$  pistons cut at  $45^\circ$  to the maximum compression axis. We used H.W.G.'s four-post high-pressure modified Griggs deformation apparatus in the Tectonophysics Laboratory of the University of California, Riverside, which is capable of controlled deformation with accurate stress measurement to pressures in excess of 3.8 GPa (ref. 25). The four-post modified Griggs apparatus is the only deformation apparatus in the world that can demonstrate low stress and achieve large shear strain above 2.5 GPa. Other high-pressure experimental facilities to conduct deformation experiments use multi-anvil apparatus, most of which are designed for hydrostatic experiments, produce very high stresses during pressurization and for which stresses during deformation cannot be measured except with synchrotron X-ray diffraction. The more recently developed Deformation-DIA apparatus also enables stress measurement with synchrotron X-ray diffraction but there remain serious ambiguities associated with stress measurement by this technique and achieving large strains has not been accomplished.

CsCl, an extremely weak solid, was used as the confining medium. All precautions were taken to maximize dryness while preparing and putting together the sample assembly. The samples were designed to produce simple shear, as described in Jung *et al.*<sup>5</sup> (although rotation of the upper  $\text{Al}_2\text{O}_3$  piston during deformation can occasionally induce a component of specimen-normal shortening to large-strain specimens—as may have happened to the 3.6 GPa specimen of this

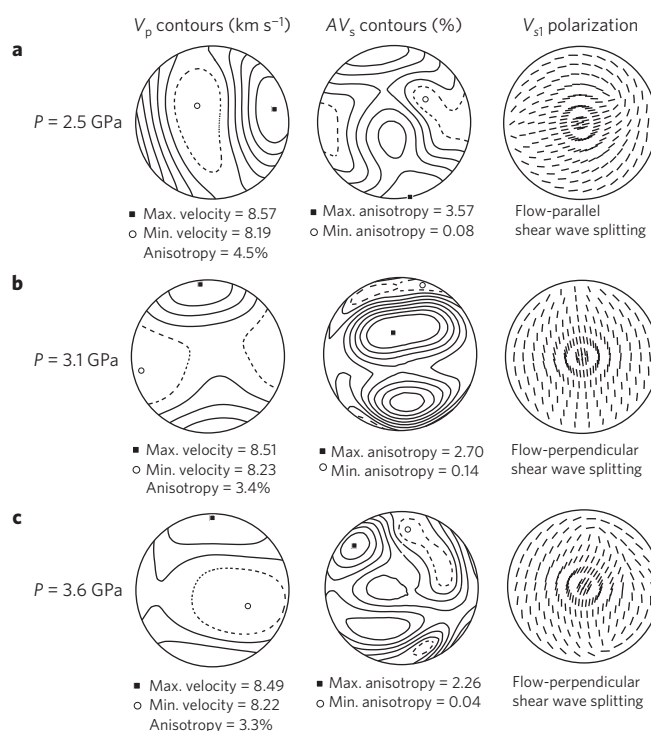


**Figure 4 | Seismic anisotropy calculated from fabrics shown in Fig. 2.** The east-west direction corresponds to the shear direction, and the centres of the diagrams correspond to the shear-plane normal (this orientation clearly shows the polarization direction of shear waves for vertically arriving seismic waves in the Earth and is different from that used in Fig. 2).  $P$ -wave seismic velocity ( $V_p$ ) and the  $S$ -wave polarization anisotropy ( $AV_s$ ) are shown.  $V_{p1}$  is a plot of the polarization direction of fast  $S$ -waves along different orientations of propagation; the centre of the figure corresponds to vertical propagation. Seismic anisotropy at  $P = 2.5$  GPa is significantly different from that at  $P = 3.1$  GPa and above.

study). We enclosed a single crystal of olivine in its strongest orientation ([010] axis parallel to the maximum principal stress) within each sample capsule to determine quantitatively the water content after each experiment.

We conducted four deformation experiments in the range 2.5–3.6 GPa, all at a temperature of  $1,300^\circ\text{C}$  at low stress, low water content and large shear strain; temperature was measured by two B-type thermocouples located near the top and bottom of the specimen. Experiments were conducted in the following manner. The pressure was increased first, followed by the temperature until the desired run conditions were obtained. The samples were deformed at a constant strain rate of  $2\text{--}6 \times 10^{-5}\ \text{s}^{-1}$ . Stress was measured with a load cell external to the apparatus; total friction in the system was measured by the force level on the moving (deformation) piston just before it encountered the specimen. As a consequence, the reported strengths are upper bounds. Stress accuracy is estimated to be  $\pm 25$  MPa; uncertainties in precision of about 5 MPa result from apparatus noise<sup>25</sup>. The shear strain,  $\gamma = \tan\theta$ , was measured in terms of the rotation angle ( $\theta$ ) of a Ni foil that was initially perpendicular to the shear plane<sup>5</sup>. Large shear strains of  $\gamma = 3\text{--}6$  ( $\pm 0.3\text{--}0.5$ ) were achieved in all cases. A small pressure increase (less than 0.1 GPa) occurred in all specimens during deformation. Oxygen fugacity was controlled by Ni/NiO similar to the previous study<sup>4</sup> by using Ni foil at the top and bottom of the sample and a Ni sleeve surrounding the sample. Detailed procedures of the deformation experiments using this apparatus are presented in Jung *et al.*<sup>26</sup>.

The CPO of olivine was measured by electron back-scatter diffraction (EBSD; using the HKL system with Channel 5 software) at an accelerating voltage of 20 kV and a working distance of 15 mm in the scanning electron microscope of the School of Earth and Environmental Sciences (SEES), Seoul National University, Korea. Each sample was scanned in a grid pattern with a step size approximately equal to the mean grain size. At each point, the EBSD pattern was indexed manually to obtain an accurate solution. We measured the CPO of  $\sim 200\text{--}460$  grains of olivine for each sample. The water content of olivine was measured on doubly polished sections ( $\sim 200\ \mu\text{m}$  thick) using a Nicolet Fourier-transform infrared (FTIR) 6700 spectrometer with a continuum infrared microscope at the Tectonophysics Laboratory of the SEES. We used an infrared beam size of

30  $\mu\text{m}$   $\times$  30  $\mu\text{m}$  without including grain boundaries. N<sub>2</sub> gas was flushed through both the infrared chamber and microscope to remove atmospheric moisture. Following Jung and Karato<sup>4</sup>, Paterson's calibration<sup>27</sup> was used to calculate the amount of water. The same data using the Bell *et al.*<sup>28</sup> calibration would yield a value  $\sim$ 3.5 times higher. The seismic wave velocity and the seismic anisotropy (Fig. 4) were calculated<sup>29</sup> from the orientation data of olivine by using the elastic constants of olivine<sup>30</sup>.

Received 1 August 2008; accepted 18 November 2008;  
published online 21 December 2008

## References

- Nicolas, A. & Christensen, N. I. *Formation of Anisotropy in Upper Mantle Peridotites—A Review* (AGU, 1987).
- Ben Ismail, W. & Mainprice, D. An olivine fabric database: An overview of upper mantle fabrics and seismic anisotropy. *Tectonophysics* **296**, 145–157 (1998).
- Park, J. & Levin, V. Geophysics—Seismic anisotropy: Tracing plate dynamics in the mantle. *Science* **296**, 485–489 (2002).
- Jung, H. & Karato, S. Water-induced fabric transitions in olivine. *Science* **293**, 1460–1463 (2001).
- Jung, H. *et al.* Effect of water and stress on the lattice-preferred orientation of olivine. *Tectonophysics* **421**, 1–22 (2006).
- Katayama, I., Jung, H. & Karato, S. I. New type of olivine fabric from deformation experiments at modest water content and low stress. *Geology* **32**, 1045–1048 (2004).
- Mizukami, T., Wallis, S. R. & Yamamoto, J. Natural examples of olivine lattice preferred orientation patterns with a flow normal a-axis maximum. *Nature* **427**, 432–436 (2004).
- Skemer, P., Katayama, I. & Karato, S. I. Deformation fabrics of the Cima di Gagnone peridotite massif, Central Alps, Switzerland: Evidence of deformation at low temperatures in the presence of water. *Contrib. Mineral. Petrol.* **152**, 43–51 (2006).
- Jung, H. Deformation fabrics of olivine in Val Malenco peridotite found in Italy and implications for the seismic anisotropy in the upper mantle. *Lithos* doi:10.1016/j.lithos.2008.06.007 (2008, in the press).
- Katayama, I., Karato, S. I. & Brandon, M. Evidence of high water content in the deep upper mantle inferred from deformation microstructures. *Geology* **33**, 613–616 (2005).
- Nakajima, J. & Hasegawa, A. Shear-wave polarization anisotropy and subduction-induced flow in the mantle wedge of northeastern Japan. *Earth Planet. Sci. Lett.* **225**, 365–377 (2004).
- Long, M. D. & van der Hilst, R. D. Upper mantle anisotropy beneath Japan from shear wave splitting. *Phys. Earth Planet. Inter.* **151**, 206–222 (2005).
- Couvy, H. *et al.* Shear deformation experiments of forsterite at 11 GPa–1400 °C in the multi-anvil apparatus. *Eur. J. Mineral.* **16**, 877–889 (2004).
- Raterron, P. *et al.* Pressure-induced slip-system transition in forsterite: Single-crystal rheological properties at mantle pressure and temperature. *Am. Mineral.* **92**, 1436–1445 (2007).
- Mainprice, D. *et al.* Pressure sensitivity of olivine slip systems and seismic anisotropy of Earth's upper mantle. *Nature* **433**, 731–733 (2005).
- Karato, S. I., Jung, H., Katayama, I. & Skemer, P. Geodynamic significance of seismic anisotropy of the upper mantle: New insights from laboratory studies. *Annu. Rev. Earth Planet. Sci.* **36**, 59–95 (2008).
- Zhang, S. Q. & Karato, S. Lattice preferred orientation of olivine aggregates deformed in simple shear. *Nature* **375**, 774–777 (1995).
- Katayama, I. & Karato, S. Effect of temperature on the B- to C-type olivine fabric transition and implication for flow pattern in subduction zones. *Phys. Earth Planet. Inter.* **157**, 33–45 (2006).
- Goetze, C. The mechanisms of creep in olivine. *Phil. Trans. R. Soc. Lond. A* **288**, 99–119 (1978).
- Long, M. D. & Silver, P. G. The subduction zone flow field from seismic anisotropy: A global view. *Science* **319**, 315–318 (2008).
- Peyton, V. *et al.* Mantle flow at a slab edge: Seismic anisotropy in the Kamchatka region. *Geophys. Res. Lett.* **28**, 379–382 (2001).
- Russo, R. M. & Silver, P. G. Trench-parallel flow beneath the Nazca plate from seismic anisotropy. *Science* **263**, 1105–1111 (1994).
- Dobrzhinetskaya, L., Green, H. W. & Wang, S. Alpe Arami: A peridotite massif from depths of more than 300 kilometers. *Science* **271**, 1841–1845 (1996).
- Jin, D. H. *Deformation Microstructures of Some Ultramafic Rocks*. MS thesis, Univ. of Minnesota, 1 (1995).
- Tingle, T. N., Green, H. W., Young, T. E. & Kocynski, T. A. Improvements to Griggs-type apparatus for mechanical testing at high-pressures and temperatures. *Pure Appl. Geophys.* **141**, 523–543 (1993).
- Jung, H., Green, H. W. & Dobrzhinetskaya, L. F. Intermediate-depth earthquake faulting by dehydration embrittlement with negative volume change. *Nature* **428**, 545–549 (2004).
- Paterson, M. S. The determination of hydroxyl by infrared absorption in quartz, silicate glasses and similar materials. *Bull. Mineral.* **105**, 20–29 (1982).
- Bell, D. R. *et al.* Hydroxide in olivine: A quantitative determination of the absolute amount and calibration of the IR spectrum. *J. Geophys. Res.—Solid Earth* **108**, 2105 (2003).
- Mainprice, D. A fortran program to calculate seismic anisotropy from the lattice preferred orientation of minerals. *Comput. Geosci.* **16**, 385–393 (1990).
- Abramson, E. H., Brown, J. M., Slutsky, L. J. & Zaugg, J. The elastic constants of San Carlos olivine to 17 GPa. *J. Geophys. Res.—Solid Earth* **102**, 12253–12263 (1997).

## Acknowledgements

We thank S. Karato, Z. Liu, P. G. Silver and J. Zhang for helpful discussions, F. Forgit for providing technical assistance during the preparation of the sample assemblies and D. Mainprice for an excellent constructive review. This work was supported by the Korea Meteorological Administration Research and Development Program under Grant CATER 2008–5112 (H.J.), and partially by the BK21 at SEES, SNU. Experimental work in H.W.G.'s laboratory was supported by NSF grants EAR-0552011 and EAR-0652960.

## Author contributions

H.J. and H.W.G. conceived the idea. H.J. conducted the high-pressure experiments. H.J. and W.M. analysed the CPO of olivine using EBSD and the water content of olivine using FTIR. H.J. wrote the first draft; H.W.G. revised it extensively. All authors discussed the results and commented on the manuscript.

## Additional information

Supplementary Information accompanies this paper on [www.nature.com/naturegeoscience](http://www.nature.com/naturegeoscience). Reprints and permissions information is available online at <http://npg.nature.com/reprintsandpermissions>. Correspondence and requests for materials should be addressed to H.J. or H.W.G.